

Detecting non-Markovian plasmonic band gaps in quantum dots using electron transport

Yueh-Nan Chen,^{1,*} Guang-Yin Chen,² Ying-Yen Liao,³ Neill Lambert,⁴ and Franco Nori^{4,5}

¹Department of Physics and National Center for Theoretical Sciences, National Cheng-Kung University, Tainan 701, Taiwan

²Institute of Physics, National Chiao Tung University, Hsinchu 300, Taiwan

³Department of Applied Physics, National University of Kaohsiung, Kaohsiung 811, Taiwan

⁴Advanced Science Institute, The Institute of Physical and Chemical Research (RIKEN), Saitama 351-0198, Japan

⁵Department of Physics and Center for Theoretical Physics, The University of Michigan, Ann Arbor, Michigan 48109-1040, USA

(Received 18 February 2009; revised manuscript received 21 May 2009; published 16 June 2009)

Placing a quantum dot close to a metal nanowire leads to drastic changes in its radiative decay behavior because of evanescent couplings to surface plasmons. We show how two non-Markovian effects, band edge and retardation, could be observed in such a system. Combined with a quantum-dot *p-i-n* junction, these effects could be readout via current-noise measurements. We also discuss how these effects can occur in similar systems with restricted geometries, such as phononic cavities and photonic crystal waveguides. This work links two previously separate topics: surface plasmons and current-noise measurements.

DOI: [10.1103/PhysRevB.79.245312](https://doi.org/10.1103/PhysRevB.79.245312)

PACS number(s): 73.20.Mf, 42.50.Pq

I. INTRODUCTION AND MOTIVATION

When a photon strikes a metal surface, a surface-plasmon polariton (a surface electromagnetic wave that is coupled to plasma oscillations) can be excited. The concept of plasmonics,¹ in analogy to photonics, has arisen as a new and exciting field since surface plasmons reveal strong analogies to light propagation in conventional dielectric components² and provide a possible miniaturization of existing photonic circuits.³

In a related context, a complete understanding of the dynamics of quantum systems interacting with their surroundings has become desirable, particularly with respect to applications for quantum information science. While the Markovian approximation is widely adopted to treat decoherence and relaxation problems, the non-Markovian dynamics of qubit (two-level) systems have come under increased scrutiny.⁴ This is because a simple Markovian description is not adequate when the qubit is strongly coupled to its environment. In solid-state systems, an exciton in a quantum dot (QD) can be viewed as such a two-level system. Recently single-qubit gate operations on QD excitons have been studied experimentally.⁵ Furthermore, with advances in fabrication technologies, it is now possible to embed QDs inside a *p-i-n* structure,⁶ such that electrons and holes can be injected separately from opposite sides. This allows one to examine the exciton dynamics in a QD via electrical currents.⁷

Motivated by these recent developments in plasmonics and quantum information science, we show in this work how non-Markovian interactions between QD excitons and nanowire surface plasmons give rise to two interesting effects: band edge and retardation. In a different system, the band-edge effect was originally predicted using the isotropic band-edge model:⁸ the quadratic dispersion relation,

$$\omega_k = \omega_c + A(k - k_c)^2,$$

leads to a photonic density-of-state $\rho(\omega)$ at a band-edge ω_c , which behaves as $1/\sqrt{\omega - \omega_c}$ for $\omega \geq \omega_c$. In a nanowire, the band-edge effect stems from the nonlinear behavior of the plasmon-dispersion relation, in which there are similar qua-

dratic local extremes at certain frequencies. The other effect we investigate here, retardation, is the multiple time delay of emission and absorption of plasmons between two QDs. With the incorporation of the system inside a *p-i-n* junction, we show that both effects can be readout via current-noise measurements. The possibility of observing such phenomena in a QD spin qubit confined in a *phononic* cavity or a QD in a *photonic* crystal waveguide are also discussed.

II. BAND-EDGE EFFECT

Consider now a semiconductor QD near a cylindrical metallic (we will consider silver here) nanowire with radius a and longitudinal axis z as shown in Fig. 1. The QD and nanowire are assumed to be separated by a dielectric layer.⁹ The n -th surface-plasmon mode's components of the electromagnetic field at the surface can be obtained by solving Maxwell's equations in a cylindrical geometry (ρ and φ denote the radial and azimuthal coordinates, respectively) with appropriate boundary conditions.¹⁰ The dispersion relations of the surface plasmons can be obtained by numerically solving the following transcendental equation:

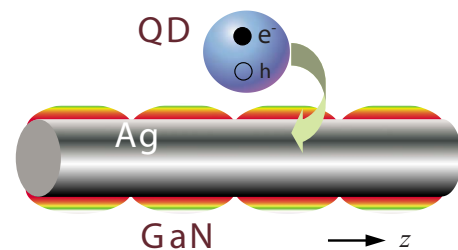


FIG. 1. (Color online) Schematic view of the system: a metallic (e.g., silver here) nanowire is embedded inside a GaN matrix and a (blue) QD (quantum dot) is placed on top of it. An evanescent electromagnetic wave couples the metallic wire and the QD. The exciton in the QD (presented by the two disks) can recombine, spontaneously emitting photons (green arrow) that produce surface plasmons on the wire (illustrated by the surface effect).

$$S(k_z, \omega) = \left[\frac{\mu_I J_n'(K_I a)}{K_I a J_n(K_I a)} - \frac{\mu_O H_n^{(1)'}(K_O a)}{K_O a H_n^{(1)}(K_O a)} \right] \times \left[\frac{(\omega/c)^2 \epsilon_I(\omega) J_n'(K_I a)}{\mu_I K_I a J_n(K_I a)} - \frac{(\omega/c)^2 \epsilon_O(\omega) H_n^{(1)'}(K_O a)}{\mu_O K_O a H_n^{(1)}(K_O a)} \right] - n^2 k_z^2 \left[\frac{1}{(K_O a)^2} - \frac{1}{(K_I a)^2} \right]^2 = 0, \quad (1)$$

whose solutions are the dispersion-relations $\omega_n = \omega_n(k_z)$. Here, $I(O)$ stands for the component inside (outside) the wire. Also, $J_n(K_I \rho)$ are $H_n^{(1)}(K_O \rho)$ are the Bessel and Hankel functions, respectively. The dielectric function is assumed as

$$\epsilon(\omega) = \epsilon_\infty \left[1 - \frac{\omega_p^2}{\omega(\omega + i/\tau)} \right], \quad (2)$$

where $\epsilon_\infty = 9.6$ (for Ag), $\epsilon_\infty = 5.3$ (for GaN), ω_p is the plasma frequency, and τ is the relaxation time due to ohmic metal loss.¹¹ The magnetic permeabilities μ_I and μ_O are unity everywhere since here we consider nonmagnetic materials. The reason to choose a silver nanowire here is that the plasmon-energy $\hbar\omega_p$ of bulk silver is 3.76 eV with the corresponding saturation-energy $\hbar\omega_p/\sqrt{2} \approx 2.66$ eV in the dispersion relation. As we shall see below, variations in the dispersion relations in energy just match the exciton band gap of wide-band-gap nitride semiconductor QDs. In related work, Gallium nitride is used as a matrix interface between a silver film and an indium gallium-nitride quantum well.¹² This is primarily because the refractive index of GaN reduces the surface-plasmon energy to match that of the exciton energy.

The dispersion relations for various modes n are shown in Fig. 2(a) with effective radius $R=0.1$. The unit of the effective radius R ($\equiv \omega_p a/c$) is roughly equal to 53.8 nm. The behavior of the $n=0$ mode is very similar to the two-dimensional case,¹³ i.e., Ω gradually saturates with increasing wave-vector k_z . This is because the fields for the $n=0$ mode are independent of the azimuthal angle φ . However, the behavior for the $n \neq 0$ modes is quite different. The first interesting point is the discontinuities around $\omega/c \approx k_z$. Further analysis shows that the solutions of ω are ‘‘almost real’’¹⁴ when $k_z > \text{Re}[\omega]/c$. Thus, the first Hankel function of order n , $H_n^{(1)}(K_O \rho)$, decays exponentially. This means that the surface plasmons in this regime are confined to the surface (*bound modes*). For $k_z < \text{Re}[\omega]/c$, however, the solutions of ω are *complex*, as shown by the dashed lines in Fig. 2(b). $H_n^{(1)}(K_O \rho)$ in this case is like a traveling wave with finite lifetime (*nonbound modes*).

A. Spontaneous emission rates

Once the electromagnetic fields are determined, the spontaneous emission (SE) rate, Γ_{SE} , of the QD excitons into bound surface plasmons can be obtained via Fermi’s golden rule. The SE rates of the first few modes ($n=0, 1, 2, 3$) are shown in Fig. 2(c) with effective radii $R=0.1$. In plotting the

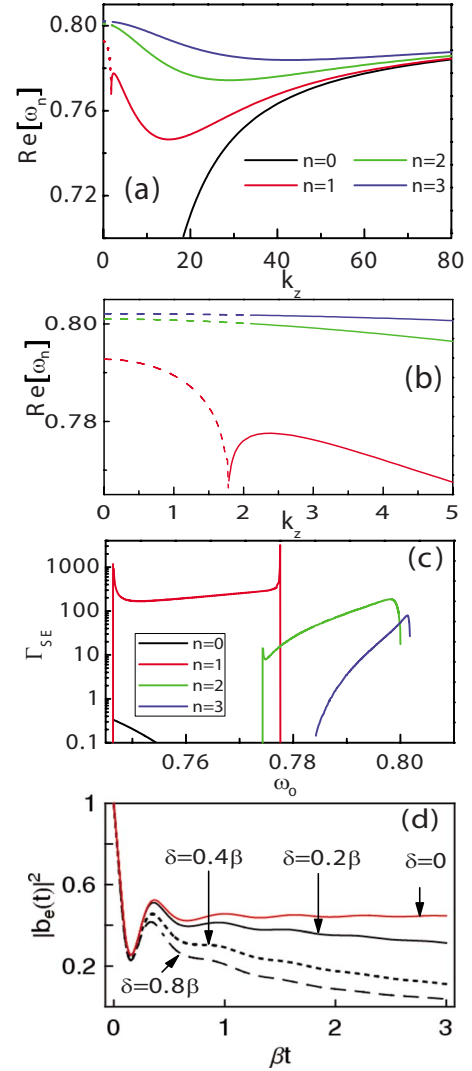


FIG. 2. (Color online) (a) Dispersion-relations $\text{Re}[\omega_n]$ vs K_z of surface plasmons for the first few modes ($n=0, 1, 2, 3$). The units for the vertical and horizontal lines are $\Omega = \omega/\omega_p$ and $K = k_z c/\omega_p$. (b) The enlarged plot of the dispersion relations of (a) in the regime of small k_z . (c) Corresponding (Markovian) spontaneous emission (SE) rates into surface plasmons. As seen here, the SE rates are greatly enhanced at certain values of ω_0 . (d) Non-Markovian decay dynamics of QD excitons for $\delta=0.2\beta$ (black line), 0.4β (dotted line), and 0.8β (dashed line). When $\delta=0$, the red (gray) curve represents the result of the contribution from the $n=1$ mode.

figures, the distance between the dot and the wire surface is fixed as $d=10.76$ nm. The novel feature is that the SE rate approaches infinity at certain values of the exciton band-gap ω_0 . Mathematically, one might think that at these values the corresponding slopes of the dispersion relation are zero. Physically, however, this infinite rate is not reasonable since it is based on perturbation theory. Therefore, one has to treat the dynamics of the exciton around these values more carefully, i.e., the *Markovian* SE rate is not enough. One has to consider the *non-Markovian* behavior around the band edge, which means the band abruptly appears/disappears across certain values of ω .

B. Non-Markovian dynamics

To obtain the non-Markovian dynamics of the exciton, we first write down the Hamiltonian of the system in the interaction picture (within the rotating wave approximation),

$$H_{\text{ex-sp}}(t) = \hbar \sum_{n,k_z} (g_{n,k_z} \hat{a}_{n,k_z}^\dagger \sigma_{\downarrow\uparrow} e^{-i\Delta_{n,k_z} t} + g_{n,k_z}^* \hat{a}_{n,k_z} \sigma_{\uparrow\downarrow} e^{i\Delta_{n,k_z} t}), \quad (3)$$

where $\sigma_{ij} = |i\rangle\langle j|$ ($i, j = \uparrow, \downarrow$) are the atomic operators; \hat{a}_{n,k_z} and \hat{a}_{n,k_z}^\dagger are the radiation-field (surface plasmon) annihilation and creation operators;

$$\Delta_{n,k_z} = \omega_n(k_z) - \omega_0 \quad (4)$$

is the detuning of the radiation-mode frequency $\omega_n(k_z)$ from the excitonic resonant-frequency ω_0 , and $g_{n,k_z} = \vec{d}_0 \cdot \vec{E}_{n,k_z}$ is the atomic field coupling. Here, \vec{d}_0 and \vec{E}_{n,k_z} denote the transition dipole moment of the exciton and the electric field, respectively. The subindex “ex-sp” in $H_{\text{ex-sp}}$ refers to excitons (ex) and surface plasmons (sp).

Assuming that initially there is an exciton in the dot with no plasmon excitation in the wire, the time-dependent wave function of the system then has the form

$$|\psi(t)\rangle = b_e(t) |\uparrow, 0\rangle + \sum_{n,k_z} b_{n,k_z}(t) |\downarrow, 1_{n,k_z}\rangle e^{-i\Delta_{n,k_z} t}. \quad (5)$$

The state vector $|\uparrow, 0\rangle$ describes an exciton in the dot and no plasmons present, whereas $|\downarrow, 1_{n,k_z}\rangle$ describes the exciton recombination and a surface plasmon emitted into mode k_z . With the time-dependent Schrödinger equation, the solution of the coefficient $b_e(t)$ in z space is straightforwardly given by

$$\tilde{b}_e(z) = \left\{ z + \sum_{n,k_z} g_{n,k_z} g_{n,k_z}^* \frac{1}{z + i[\omega_n(k_z) - \omega_0]} \right\}^{-1}. \quad (6)$$

In principle, $b_e(t)$ can be obtained by performing an inverse Laplace transformation to Eq. (6). For the usual Markovian case, $\omega_n(k_z)$ is a linear function of k_z . One can easily apply the pole approximation to Eq. (6) and obtain the exponential decay behavior of $b_e(t)$. However, as shown in Fig. 2(a), the dispersion curves for $n=1, 2$, and 3 , are nonlinear near their minima, which thus give a clear interpretation for the detuning Δ_{n,k_z} in Eq. (3): the energy difference between ω_0 and the minimum. This implies that the group velocity of the surface plasmons, $v_g = \partial\omega_n(k_z)/\partial k_z$, is zero at the minimum point, and the pole approximation is not valid there.

To grasp the main physics and without loss of generality, we focus on the values of ω_0 close to one particular local extremum (maximum or minimum), where the dispersion relation for a particular mode becomes quadratic. In this case, the dispersion relation for this particular mode around the extreme can be approximated as

$$\omega_n(k_z) = \omega_{n,c} \pm A_n(k_z - k_{n,c})^2, \quad (7)$$

where the extremum is located at $(k_{n,c}, \omega_{n,c})$. The $+/-$ sign represents the approximate curve for the local minimum/maximum of the dispersion relation. Once we make such an

approximation, the radiative dynamics of the QD exciton is just like that of a two-level atom in a photonic crystal^{8,15} with

$$\tilde{b}_e(z) \approx \frac{|\vec{d}_0 \cdot \vec{E}_{n,k_z=k_{n,c}}|^2}{z - \gamma/2 - \frac{(-1)^{3/4}\pi}{\sqrt{A_n}\sqrt{z-i\delta}}}, \quad \text{for local minima} \quad (8)$$

$$\tilde{b}_e(z) \approx \frac{|\vec{d}_0 \cdot \vec{E}_{n,k_z=k_{n,c}}|^2}{z - \gamma/2 + \frac{(-1)^{1/4}\pi}{\sqrt{A_n}\sqrt{z-i\delta}}}, \quad \text{for local maxima} \quad (9)$$

where

$$\delta = \omega_0 - \omega_{n,c}$$

is the detuning to a specific extremum and γ is the decay rate contributed from other modes. For example, hereafter we choose ω_0 to be close to the minimum of the $n=1$ mode, and thus only this $n=1$, and the $n=0$ mode, strongly interact with the exciton. The other modes can be treated as a (Markovian) decay process with a rate γ .

The coefficient $b_e(t)$ can now be obtained^{8,15} by performing the Laplace transformation to Eqs. (8) and (9). The black, dotted, and dashed lines in Fig. 2(d) represent the decay dynamics of the QD excitons for different detunings: $\delta=0.2\beta$, 0.4β , and 0.8β , respectively. Here, β is the decay rate of the QD exciton in free space. As mentioned above, when plotting Fig. 2(d), ω_0 was chosen to be close to the local minimum of the dispersion relation of the $n=1$ mode. The radius of the wire and the wire-dot separation are identical to those in Fig. 2(a). As can be seen in Fig. 2(d), there exists oscillatory behavior in the decay profile of $|b_e(t)|^2$, demonstrating that the decay dynamics around the local extrema is non-Markovian. If one only considers the contribution from the $n=1$ mode and set the detuning $\delta=0$, the probability amplitude would saturate to a steady limit, as shown by the top red (gray) curve in Fig. 2(d). This *quasidressed* state is reminiscent of damped Rabi oscillations in cavity quantum electrodynamics, and also appears in systems of photonic crystals.^{8,15}

C. Readout of the band-edge effect via current-noise

With recent advances in fabrication technologies, it is now possible to embed QDs inside a p - i - n structure.⁶ Furthermore, the interest in measurements of shot noise in quantum transport has grown recently owing to the possibility of extracting valuable information not available in conventional dc transport experiments.¹⁶ We thus propose to bring these two branches of condensed-matter physics together: surface-plasmon and current-noise measurements; i.e., by placing a QD p - i - n junction close to the nanowire as shown in Fig. 3.

In addition to the Hamiltonian $H_{\text{ex-sp}}$ in Eq. (3), we now need to consider the tunnel couplings to the electron and hole reservoirs,⁷

$$H_T = \sum_{\mathbf{q}} (V_{\mathbf{q}} c_{\mathbf{q}}^\dagger |0\rangle\langle\uparrow| + W_{\mathbf{q}} d_{\mathbf{q}}^\dagger |0\rangle\langle\downarrow| + \text{H.c.}), \quad (10)$$

where $c_{\mathbf{q}}$ and $d_{\mathbf{q}}$ are the electron operators in the right and left reservoirs, respectively. Here, $V_{\mathbf{q}}$ and $W_{\mathbf{q}}$ couple the

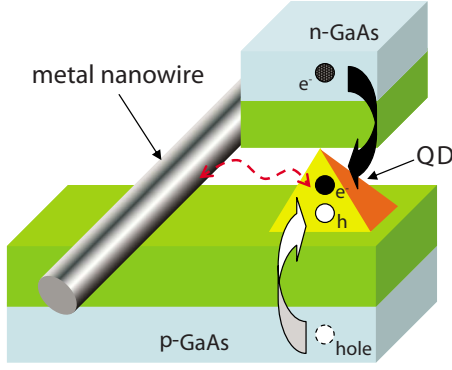


FIG. 3. (Color online) A schematic diagram of a *p-i-n* junction with a quantum dot (QD) evanescently coupled to surface plasmons in a nanowire.

channels \mathbf{q} of the electron and the hole reservoirs. We also introduced the three dot states: $|0\rangle = |0, h\rangle$, $|\uparrow\rangle = |e, h\rangle$, and $|\downarrow\rangle = |0, 0\rangle$, where $|0, h\rangle$ means that there is one hole in the QD, $|e, h\rangle$ is the exciton state, and $|0, 0\rangle$ represents the ground state with no hole and no excited electron in the QD.⁷

Together with Eq. (3), one can now write down the equation of motion for the reduced density operator

$$\begin{aligned} \frac{d}{dt}\rho(t) = & -\text{Tr}_{\text{res}} \int_0^t dt' \{H_T(t) + H_{\text{ex-sp}}(t), [H_T(t') \\ & + H_{\text{ex-sp}}(t'), \tilde{\Xi}(t')]\}, \end{aligned} \quad (11)$$

where $\tilde{\Xi}(t')$ is the total density operator. Note that the trace, Tr , in Eq. (11) is taken with respect to both plasmon and electronic reservoirs. If the couplings to the electron and hole reservoirs are weak, it is reasonable to assume that the standard Born-Markov approximation with respect to the electronic couplings is valid. Without making the Markovian approximation to the exciton-plasmon couplings, one can obtain a closed equation for the reduced density operators by tracing out the electron and plasmon reservoirs,¹⁷

$$\begin{aligned} \frac{d}{dt}\rho(t) = & -\int_0^t dt' \sum_{n, k_z} |g_{n, k_z}|^2 \{[\sigma_{\uparrow\downarrow} \sigma_{\downarrow\uparrow} \rho(t') - \sigma_{\downarrow\uparrow} \rho(t') \sigma_{\uparrow\downarrow}] \\ & \times e^{i\Delta_{n, k_z}(t-t')} + \text{H.c.}\} - \Gamma_L \int_0^t dt' \{s_L(t') s_L^\dagger(t') \rho(t') \\ & - 2s_L^\dagger(t') \rho(t') s_L(t')\} - \Gamma_L \int_0^t dt' \{\rho(t') s_L(t') s_L^\dagger(t')\} \\ & - \Gamma_R \int_0^t dt' \{s_R^\dagger(t') s_R(t') \rho(t')\} \\ & - \Gamma_R \int_0^t dt' \{\rho(t') s_R^\dagger(t') s_R(t') - 2s_R(t') \rho(t') s_R^\dagger(t')\}, \end{aligned} \quad (12)$$

where $s_L = |0\rangle\langle\uparrow|$, and $s_R = |0\rangle\langle\downarrow|$, denote the tunneling operators, and Γ_L (Γ_R) is the tunneling rate from the electron (hole) reservoir.

To study correlations between carriers, we relate the exciton dynamics with the hole-reservoir operators by introducing a counting variable n , defined as the number of holes that have tunneled through the hole-side barrier, and expectation values, $O^{(n)} \equiv \sum_{i=0, \uparrow, \downarrow} \text{Tr}_{\text{bath}} \langle n, i | \hat{O} \rho(t) | n, i \rangle$, with $\langle \hat{O} \rangle = \sum_n O^{(n)}$. This leads to a system of equations of motion,

$$\begin{aligned} \frac{dn_0^{(n)}(t)}{dt} = & -\Gamma_L n_0^{(n)}(t) + \Gamma_R n_{\downarrow}^{(n-1)}(t), \\ \frac{dn_{\uparrow}^{(n)}(t)}{dt} + \frac{dn_{\downarrow}^{(n)}(t)}{dt} = & (\Gamma_L - \Gamma_R) n_0^{(n)}(t), \end{aligned} \quad (13)$$

where Eq. (13) allows us to calculate the particle current and the noise spectrum from

$$P_n(t) = n_0^{(n)}(t) + n_{\uparrow}^{(n)}(t) + n_{\downarrow}^{(n)}(t),$$

which gives the total probability of finding n electrons in the collector by time t . In particular, the noise spectrum S_{I_R} can be calculated via the MacDonald formula,

$$S_{I_R}(\omega) = 2\omega e^2 \int_0^\infty dt \sin(\omega t) \frac{d}{dt} [\langle n^2(t) \rangle - (t\langle I \rangle)^2], \quad (14)$$

where $\frac{d}{dt} \langle n^2(t) \rangle = \sum_n n^2 \dot{P}_n(t)$. With the help of counting statistics,¹⁶ the noise spectrum is then given by

$$S_{I_R}(\omega) = 2eI \{1 + \Gamma_R [B(\omega) + B(-\omega)]\}, \quad (15)$$

where

$$B(\omega) = \frac{A(i\omega)\Gamma_L}{-A(i\omega)\Gamma_L\Gamma_R + [A(i\omega) + i\omega](\Gamma_L + i\omega)(\Gamma_R + i\omega)}. \quad (16)$$

Here, I is the stationary current, and $A(z) \equiv c(z) + c^*(z)$, where

$$c(z) = \sum_{n, k_z} \frac{g_{n, k_z} g_{n, k_z}^*}{z + i[\omega_n(k_z) - \omega_0]}. \quad (17)$$

Figure 4(a) shows the noise-spectrum $S_{I_R}(\omega)$ as a function of ω . As for Fig. 2(d), the value of ω_0 here is chosen to be close to the local minimum of the $n=1$ mode. Here, the Γ_L and Γ_R are set equal to 0.01β and 0.1β , respectively. The solid (dashed) line represents the result for a detuning of $\delta = \omega_0 - \omega_{n,c} = -0.01\beta$ (0.01β). The interesting feature here is that there are discontinuities at $\omega = \pm 0.01\beta$. For the case of $\delta = -0.01\beta$, the Poissonian value of the noise spectrum [$S_{I_R}(\omega) = 1$ for $-0.01\beta < \omega < 0.01\beta$] is analogous to that of putting a two-level emitter inside the band gap, while, for $\delta = 0.01\beta$, the sub-Poissonian value is the situation outside the band gap.¹⁸ Figure 4(b) shows the density plot of the noise spectrum as functions of both ω and detuning $\delta = \omega_0 - \omega_{n,c}$. As seen there, for $\delta < 0$, the values of $S_{I_R}(\omega)$ in the regime $-|\delta| < \omega < |\delta|$ are larger than those in $\omega < -|\delta|$ and $|\delta| < \omega$. For $\delta > 0$, however, it is the opposite behavior. In addition, one also observes that there are discontinuities along the lines $\delta = \pm \omega$. Together with the results in Fig. 4(a), we conclude that the feature of *discontinuities* in these noise

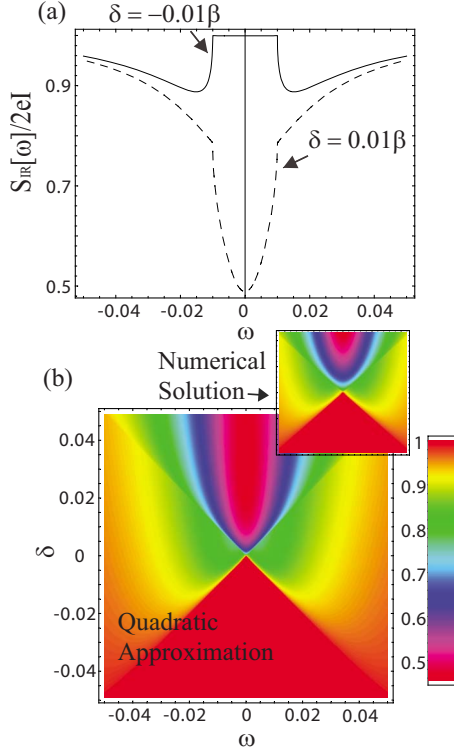


FIG. 4. (Color online) (a) Noise spectrum as a function of ω . Such as that in Fig. 2(d), the value of ω_0 here is chosen to be close to the local minimum of the $n=1$ mode. Here, Γ_L and Γ_R are set equal to 0.01β and 0.1β , respectively. The solid (dashed) line represents the result for $\delta=-0.01\beta$ (0.01β). (b) Density plot of the current-noise spectrum as functions of ω and detuning $\delta=\omega_0-\omega_{n,c}$, which are both in units of β , the decay rate of the QD in free space. As seen here, there are discontinuities along the lines $\delta=\pm\omega$, which is an indication of the band-edge effect. In the inset we show the same calculation using the numerical solution for the dispersion relation, not the quadratic approximation. This illustrates that the important features are all contained within the quadratic approximation.

spectra can actually be viewed as an indication of a band-edge effect.

III. RETARDATION EFFECT

By placing two QDs close to the nanowire, and by making use of the one-dimensional propagating feature of the nanowire surface plasmons, another non-Markovian effect, the retardation, can be observed. For simplicity, the exciton-energy $\hbar\omega_0$ of the two identical dots is set well below the local minimum of the $n=1$ mode, such that only the $n=0$ mode contributes to the decay rate. Thus, the interaction Hamiltonian can be expressed as

$$\hat{H}_I = -i\hbar \sum_{l=1,2} \sum_{k_z} (\hat{a}_{k_z} - \hat{a}_{k_z}^\dagger) \times (g_{k_z}^* e^{-ik_z z_l} |\downarrow\rangle_l \langle \uparrow| + g_{k_z} e^{ik_z z_l} |\uparrow\rangle_l \langle \downarrow|), \quad (18)$$

where z_l is the position of the l -th dot, and the distance of the two dots to the wire surface is the same. Assuming that only

dot-1 is initially excited, the state vector of the system can be written as

$$|\psi(t)\rangle = b_1(t)|\uparrow\downarrow,0\rangle + b_2(t)|\downarrow\uparrow,0\rangle + \sum_{k_z} b_{k_z}(t)|\downarrow\downarrow,1_{n,k_z}\rangle, \quad (19)$$

with the initial conditions: $b_1(0)=1$, $b_2(0)=0$, and $b_{k_z}(0)=0$. The time-dependent solutions are straightforwardly given by $b_{1(2)}(t)=[C_+(t)\pm C_-(t)]/2$, with

$$C_{\pm}(t) = \frac{1}{2\pi i} \int_{-\infty+\epsilon}^{i\infty+\epsilon} ds \frac{e^{st}}{s + \sum_{k_z} |g_{k_z}|^2 [1 \pm e^{ik_z(z_2-z_1)}] G(s)}, \quad (20)$$

where

$$G(s) = \{s + i[\omega_n(k_z) - \omega_0]\}^{-1} + \{s + i[\omega_n(k_z) + \omega_0]\}^{-1}.$$

Following the well-known treatment of retardation,¹⁹ one can obtain the probability amplitudes of the dots in the regime of $k_0 r \geq 3$,

$$b_{1(2)}(t) = \sum_{\substack{m=0,2,4,\dots \\ (m=1,3,5,\dots)}}^{\infty} \frac{1}{m!} (ie^{ik_0 r})^m \left[\gamma_0 \left(t - \frac{mr}{v} \right) \right]^m \times H \left(t - \frac{mr}{v} \right) \exp \left\{ -\gamma_0 \left(t - \frac{mr}{v} \right) \right\}, \quad (21)$$

where $r=|z_2-z_1|$, $k_0 \approx \omega_0/v$, v is the velocity of the surface plasmon on the wire, γ_0 is the SE rate of a single QD exciton into a surface plasmon, and H is the unit step function.

One might argue that the surface plasmons inevitably experience losses as they propagate along the nanowire, which could limit the feasibility of observing the retardation effect. One solution to this would be to couple two QDs to two separate nanowires. Meanwhile, the wires would be evanescently coupled to a phase-matched dielectric waveguide.²⁰ In this case, one could have both the advantages of strong coupling from the surface plasmons and also long-distance transport in the dielectric waveguide. In addition, the non-Markovian retarding effect can also be measured via current noise if one of the dots is embedded inside a p - i - n junction as shown in Fig. 5(a). Following the procedure described above, the noise spectrum is given by

$$S_{I_R}(\omega) = 2eI \{ 1 + \Gamma_R [n_R(s=-i\omega) + n_R(s=i\omega)] \}. \quad (22)$$

In Eq. (22), $n_R(s)$ is the Laplace transformation of the ground-state occupation probability $n_R(t) = \langle |\downarrow\downarrow\rangle \langle \downarrow\downarrow| \rangle_t$, where the average is over both the electronic and photonic reservoirs. The red (gray) and blue (dark gray) lines in Fig. 5(b) represent the noise spectra for $\gamma_0 r/v = 2\pi$ and 4π , respectively. As seen there, the main difference to the nonretarded case (black line) is the oscillatory behavior, which depends on the interdot-separation r . One recalls that in the nonretarded situation there should be no difference whenever $\gamma_0 r/v = m\pi$, where m is an integer.²¹ The green (light gray) line in the inset of Fig. 5(b) is the result for $\gamma_0 r/v = 1.9$. This means that even if the value of $\gamma_0 r/v$ is not equal to $m\pi$, one

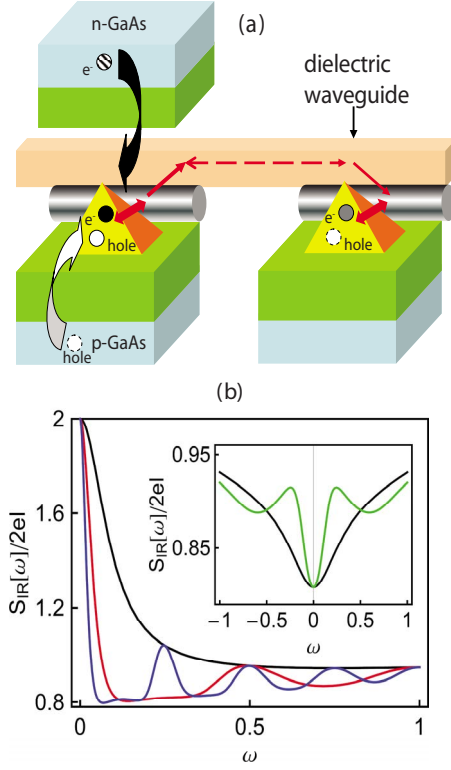


FIG. 5. (Color online) (a) Proposed device for the observation of retardation effects via current noise. The two QDs are coupled to two separate nanowires. Meanwhile, the wires are evanescently coupled to a phase-matched dielectric waveguide. (b) Current noises of the double-dot device. The red (gray) and blue (dark gray) lines represent the results for $\gamma_0 r/v=2\pi$ and 4π , respectively. Recall that r is the interdot separation. The black line is the result for the Markovian case. The most obvious feature for the non-Markovian effect is the oscillatory behavior [red (gray) and blue (dark gray) curves]. Inset: Noise spectra with [green (light gray) line] and without [black line] retardation effects when $\gamma_0 r/v=1.9$.

still could observe the predicted oscillatory behavior. One also notes that, in the case of $\gamma_0 r/v=m\pi$, the value of the Fano factor (zero-frequency noise) is twice the Poissonian value. This is because a singlet entangled state, $|\uparrow\downarrow\rangle-|\downarrow\uparrow\rangle$, may occasionally be formed during one of the transport events (electrons/holes entering and leaving the left dot). If this happens, the subradiant channel becomes the dominant one and the result is a photon-trapping phenomenon.⁷ This behavior causes an enhancement of the noise value by a factor of 2, as has been pointed out in Ref. 21.

IV. BAND-EDGE EFFECT IN PHONON CAVITIES

The non-Markovian effects studied above can also be observed in other physical systems. For example, if one considers a freestanding slab²² with width w , small elastic vibrations of a solid slab can then be defined by a vector of relative-displacement $\mathbf{u}(\mathbf{r}, t)$. Under the isotropic elastic continuum approximation, the displacement-field \mathbf{u} obeys the equation

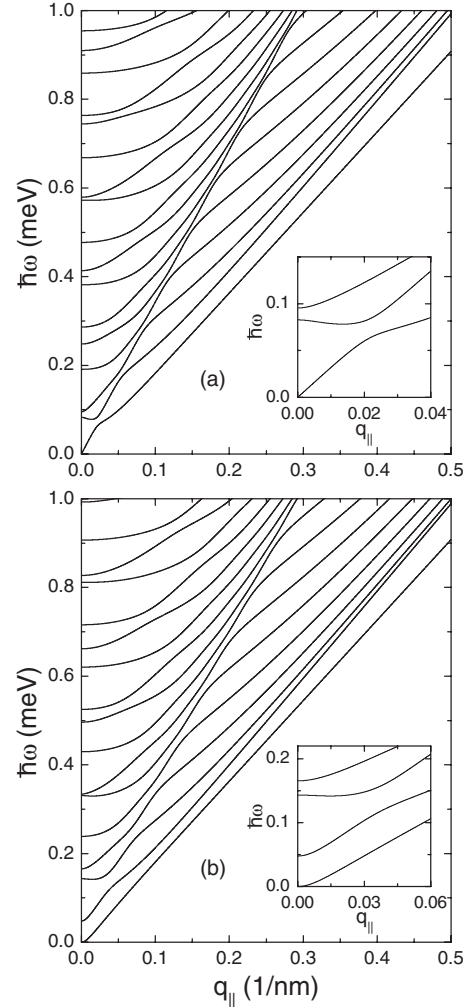


FIG. 6. Dispersion relations for (a) the dilatational waves and (b) the flexural waves in a slab with width $w=130$ nm. The insets are the corresponding magnified plots in the small q_{\parallel} regime. As can be seen here, the dispersion relations of the confined phonons also exhibit the “band-edge” feature for certain values of ω .

$$\frac{\partial^2 \mathbf{u}}{\partial t^2} = c_l^2 \nabla^2 \mathbf{u} + (c_l^2 - c_t^2) \nabla (\nabla \cdot \mathbf{u}), \quad (23)$$

where c_l and c_t are the velocities of longitudinal and transverse bulk-acoustic waves. To define a system of confined modes, Eq. (23) is complemented by the boundary conditions at the slab-surface $z=\pm w/2$. Because of the confinement, phonons will be quantized in subbands. For each in-plane component \mathbf{q}_{\parallel} of the in-plane wave vector there are infinitely many subbands. Since two types of velocities of sound exist in the elastic medium, there are also two transverse wave-vectors q_l and q_t . If one further considers the deformation potential only, then there are two main confined acoustic modes: dilatational waves and flexural waves. For dilatational waves, the parameters $q_{l,n}$ and $q_{t,n}$ can be determined from the Rayleigh-Lamb equation

$$\frac{\tan(q_{l,n}w/2)}{\tan(q_{t,n}w/2)} = -\frac{4q_{\parallel}q_{l,n}q_{t,n}}{(q_{\parallel}^2 - q_{t,n}^2)^2}, \quad (24)$$

with the dispersion relation

$$\omega_{n,q_{\parallel}} = c_l \sqrt{q_{\parallel}^2 + q_{l,n}^2} = c_t \sqrt{q_{\parallel}^2 + q_{t,n}^2}, \quad (25)$$

where $\omega_{n,q_{\parallel}}$ is the frequency of the dilatational wave in mode (n, q_{\parallel}) . For the antisymmetric flexural waves, the solutions $q_{l,n}$ and $q_{t,n}$ can also be determined by solving the equation

$$\frac{\tan(q_{l,n}w/2)}{\tan(q_{t,n}w/2)} = -\frac{4q_{\parallel}q_{l,n}q_{t,n}}{(q_{\parallel}^2 - q_{t,n}^2)^2}, \quad (26)$$

together with the dispersion relation, Eq. (25).

Figures 6(a) and 6(b) numerically show the dispersion relations for dilatational and flexural waves, respectively. As can be seen in the insets, local minima also appear in the dispersion relations. An enhanced relaxation rate due to the phonon van Hove singularities has been predicted if a double-dot charge qubit²³ or single-dot spin state²⁴ is embedded in such a phonon cavity. However, as we have mentioned above, the greatly enhanced rates are also from the band-edgelike effect,²⁵ and one should treat the dynamics of the qubits as non-Markovian. As for the retardation effect, the two QDs may also be embedded inside a well-designed photonic crystal waveguide,²⁶ in which the propagation of the photon is restricted to one dimension. In this case, the advantage of the retardation effect in one dimension is still kept, and the combination with the p - i - n junction should also be workable.¹⁸

V. CONCLUSIONS

In summary, we have shown that nanowire surface plasmons, which we consider as a bosonic reservoir with a re-

stricted geometry, have a nonlinear dispersion relation with extreme values at certain frequencies. When coupled to a QD exciton (combined with a p - i - n junction) we described how it should be possible to observe the non-Markovian dynamics of these effects when the recombination energy of the exciton is close to the band gap of the plasmon reservoir. We calculated specific results for the current-noise frequency spectrum and observed unique signatures of these “band-edge” non-Markovian dynamics.

Furthermore, we have shown that the retardation effect, another non-Markovian effect which occurs when two dots are both strongly coupled to the same nanowire, has also unique signatures in the current noise. Finally, we illustrated how these effects might also be observed in a QD spin qubit (or double-dot charge qubit) embedded inside a phonon cavity.

ACKNOWLEDGMENTS

We would like to thank J. Taylor for helpful discussions. This work is supported partially by the National Science Council, Taiwan under Grant No. 95-2112-M-006-031-MY3. F.N. acknowledges partial support from the National Security Agency (NSA), Laboratory for Physical Sciences (LPS), Army Research Office (ARO), National Science Foundation (NSF) (Grant No. EIA-0130383), JSPS-RFBR (Contract No. 06-02-91200), and CTC program supported by the Japan Society for Promotion of Science (JSPS).

*yuehnan@mail.ncku.edu.tw

¹See, e.g., S. A. Maier, *Plasmonics: Fundamentals and Applications* (Springer, New York, 2007); K. Y. Bliokh, Y. P. Bliokh, V. Freilikher, S. Savelev, and F. Nori, *Rev. Mod. Phys.* **80**, 1201 (2008).

²See, e.g., R. Zia and M. L. Brongersma, *Nat. Nanotechnol.* **2**, 426 (2007).

³See, e.g., S. I. Bozhevolnyi, V. S. Volkov, E. Devaux, J. Laluet, and T. W. Ebbesen, *Nature (London)* **440**, 508 (2006); S. Savell'ev, A. L. Rakhmanov, V. Yampol'skii, and F. Nori, *Nat. Phys.* **2**, 521 (2006).

⁴See, e.g., B. Bellomo, R. Lo Franco, and G. Compagno, *Phys. Rev. Lett.* **99**, 160502 (2007); J. Piilo, S. Maniscalco, K. Härkönen, and K.-A. Suominen, *ibid.* **100**, 180402 (2008).

⁵X. Q. Li, Y. W. Wu, D. Steel, D. Gammon, T. H. Stievater, D. S. Katzer, D. Park, C. Piermarocchi, and L. J. Sham, *Science* **301**, 809 (2003).

⁶Z. Yuan, B. E. Kardynal, R. M. Stevenson, A. J. Shields, C. J. Lobo, K. Cooper, N. S. Beattie, D. A. Ritchie, and M. Pepper, *Science* **295**, 102 (2002).

⁷See, e.g., Y. N. Chen, D. S. Chuu, and T. Brandes, *Phys. Rev. Lett.* **90**, 166802 (2003).

⁸S. John and T. Quang, *Phys. Rev. A* **50**, 1764 (1994).

⁹A. V. Akimov, A. Mukherjee, C. L. Yu, D. E. Chang, A. S.

Zibrov, P. R. Hemmer, H. Park, and M. D. Lukin, *Nature (London)* **450**, 402 (2007).

¹⁰C. A. Pfeiffer, E. N. Economou, and K. L. Ngai, *Phys. Rev. B* **10**, 3038 (1974); S. S. Martinos and E. N. Economou, *ibid.* **28**, 3173 (1983); S. S. Martinos, *ibid.* **31**, 2029 (1985).

¹¹P. B. Johnson and R. W. Christy, *Phys. Rev. B* **6**, 4370 (1972); R. Paiella, *Appl. Phys. Lett.* **87**, 111104 (2005).

¹²I. Gontijo, M. Boroditsky, E. Yablonovitch, S. Keller, U. K. Mishra, and S. P. DenBaars, *Phys. Rev. B* **60**, 11564 (1999).

¹³J. A. Stratton, *Electromagnetic Theory* (McGraw-Hill, New York, 1941).

¹⁴G. Y. Chen, Y. N. Chen, and D. S. Chuu, *Opt. Lett.* **33**, 2212 (2008).

¹⁵S.-Y. Zhu, Y. Yang, H. Chen, H. Zheng, and M. S. Zubairy, *Phys. Rev. Lett.* **84**, 2136 (2000).

¹⁶See, e.g., C. W. J. Beenakker, *Rev. Mod. Phys.* **69**, 731 (1997); Y. M. Blanter and M. Buttiker, *Phys. Rep.* **336**, 1 (2000); R. Aguado and T. Brandes, *Phys. Rev. Lett.* **92**, 206601 (2004); N. Lambert and F. Nori, *Phys. Rev. B* **78**, 214302 (2008).

¹⁷Y. N. Chen, *Appl. Phys. Lett.* **90**, 162114 (2007).

¹⁸Y. N. Chen, D. S. Chuu, and T. Brandes, *Phys. Rev. B* **72**, 153312 (2005).

¹⁹P. W. Milonni and P. L. Knight, *Phys. Rev. A* **10**, 1096 (1974).

²⁰D. E. Chang, A. S. Sørensen, E. A. Demler, and M. D. Lukin,

- Nat. Phys. **3**, 807 (2007).
- ²¹Y. N. Chen, T. Brandes, C. M. Li, and D. S. Chuu, Phys. Rev. B **69**, 245323 (2004); See also, N. Lambert, R. Aguado, and T. Brandes, *ibid.* **75**, 045340 (2007).
- ²²E. M. Weig, R. H. Blick, T. Brandes, J. Kirschbaum, W. Wegscheider, M. Bichler, and J. P. Kotthaus, Phys. Rev. Lett. **92**, 046804 (2004).
- ²³S. Debold, T. Brandes, and B. Kramer, Phys. Rev. B **66**, 041301(R) (2002).
- ²⁴Y. Y. Liao, Y. N. Chen, D. S. Chuu, and T. Brandes, Phys. Rev. B **73**, 085310 (2006).
- ²⁵S. Debold, T. Brandes, and T. Vorrath, Int. J. Mod. Phys. B **17**, 5471 (2003); G. Lindwall, A. Wacker, C. Weber, and A. Knorr, Phys. Rev. Lett. **99**, 087401 (2007).
- ²⁶S. Noda, A. Chutinan, and M. Imada, Nature (London) **407**, 608 (2000); E. Chow, S. Y. Lin, S. G. Johnson, P. R. Villeneuve, J. D. Joannopoulos, J. R. Wendt, G. A. Vawter, W. Zubrzycki, H. Hou, and A. Alleman, *ibid.* **407**, 983 (2000).